Computation of ion exchange buried microring resonator waveguide for THz communication applications

Iraj S. Amiri[a,b,*,1], F. Alizadeh[c], M.M. Ariannejad[d], R. Amini[c,2], P. Yupapin[a]

[a] Computational Optics Research Group, Advanced Institute of Materials Science, Ton Duc Thang University, Ho Chi Minh City, Viet Nam
[b] Faculty of Applied Sciences, Ton Duc Thang University, Ho Chi Minh City, Viet Nam
[c] University of Tehran (UT), 141556458 Tehran, Iran
[d] Photonics Research Centre, University of Malaya, 50603 Kuala Lumpur, Malaysia

ABSTRACT

The ion exchange creates the optical buried waveguides, whereas it is the method that the glass doping occurs with the condition of existence of the mobile metal ions. The most common ion used is silver (Ag+) due to its broad variation in the refractive index. The proposed application presented in this work is to use the microring resonator (MRR) system based on the buried waveguides simulated by the ion exchange method. The passive MRRs are realized as the multi-wavelength transceiver, applicable in optical technologies such as the optical sensing, Terahertz (THz) communication and optical switching. The cross-sectional view of the simulated buried optical waveguide for the Ag+ concentrations of $0.8 \, mol/m^3$ is presented. The fundamental mode propagation is simulated using the time-domain traveling wave method, where the simulation of the optical power flow density and the electric field distributions of the buried waveguides were performed. The two coupled MRRs are used to generate tunable dual-wavelength with spacing in the range of Terahertz (THz). As results, the dual wavelengths in the range between 0.25 and 0.96 THz were generated at the throughput and drop port of the MRRs system.

Introduction

Many research investigations have shown that the ion exchange technique is applicable to generate waveguide structures [1–3]. In order to control the absorption of the glass materials, the ion exchange can be utilized [4]. As advantages of using ion exchange technique, low optical losses are observed in waveguides, where this technique has high compatibility with optical fiber assembly [5,6]. The ions from a molten salt have the different ionic radius and polarizability from those of Na+, such as stress in the glass matrix. The silver (Ag+) is the most common ion due to broad variation in the refractive index comparable to thallium (Tl+) and potassium (K+). To reduce the fabrication difficulties for integrated optical components, which become more and more complex at present, modeling procedures accomplish an increasing interest [7]. Thin glass films, can be used as the substrate to produce buried waveguide using sol-gel coating, flame hydrolysis deposition, and chemical vapor deposition methods [8]. Several deposition steps and etching make these methods time consuming costly. The highest motivations for using the ion exchange in the glass was to use

optical waveguide as sensors, where the glass has minimal optical attenuation and it is rugged against a diversity in case of atmospheric, mechanical and thermal strains [9–12]. Glass is a multitude of forms and compositions [13,14]. The solid-state process over the molten salt ion exchange can be performed in a variety of temperatures even at low temperature, with ease of charge control process and ion uniformity. The Ag+ from the AgNO₃ together with the Na+ belong to the glass, can be melted at relatively low temperatures ranges 220–300 °C, therefore the Ag+ and Na+ exchange can be performed. Therefore, the mechanism of the ion exchange can be unselective or have binding preferences which occurs for only certain ions or classes of ions such as Ag+ and Na+. In this process, only specific ions can be exchanged depending on the material chemical structures, in which, the charge and size of the ion, have significant effects. Compared to the material absorption and adsorption, ion exchange is a form of sorption, which can be defined as the physical and chemical process by which one substance becomes attached to another. The process can be found in Ref. [1], where an optical sensing device has been realized. The refractive index variation is 0.1 for soda-lime glasses.

* Corresponding author at: Ton Duc Thang University, Ho Chi Minh City, Viet Nam.
undefinedundefined
URL: https://scholar.google.com.my/citations?user=rM8jFG4AAAAJ&hl=en (I.S. Amiri).
[1] *Email address of the corresponding author:* irajsadeghamiri@tdt.edu.vn.
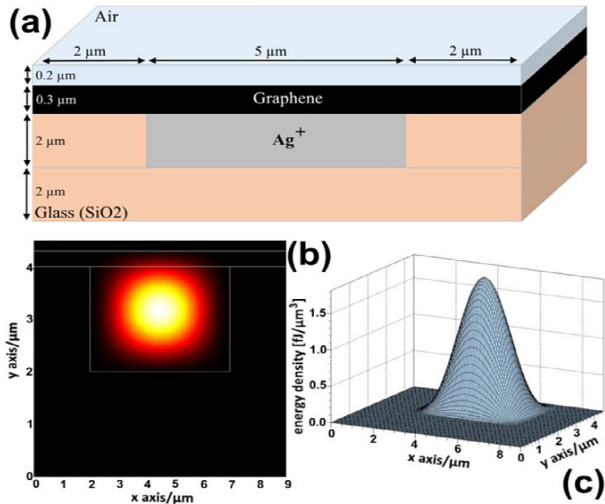[2] *Email address of co-author:* rahmatamini@ut.ac.ir.

Fig. 1. Presented structure, (a) dimensions of the proposed structure, (b) Propagating of the fundamental mode, (c) 3D image.

Simulations and methods

Ion exchange waveguide can be simulated by IONEX software. The IONEX has an algorithm to solve the differential diffusion equation base on Finite Difference Method (FDM). In this paper, we present a simple proposed design for a wavelength division multiplexing (WDM) interconnection system based on buried microring resonators (MRRs). The structure can be shown in Fig. 1.

The concentration of the Ag+ will determine the width and the depth of the channel. The more uniform surface can be obtained by controlling the concentration. With the fine surface of the waveguide, the preparation of the light along the waveguide length will have a lower loss. Fig. 1(b) presents the propagation of the fundamental mode. The method used in this study to simulate the waveguide structure of the MRRs is the time-domain traveling wave which is an efficient tool to simulate both active and passive waveguides. As shown in Table 1, the properties of the fundamental mode propagation are presented, where we have demonstrated the optical power flow density in Fig. 2(a–c). This plot is presented in three respective viewpoints namely, topside, the front side (input port) and backside (output port) for the simulated passive waveguide. Fig. 2(b) shows the incident wave view with the input center wavelength of 1.55 μm which is propagating in the normal direction to the surface of an input port of the Ag+ buried waveguide. The Ag+ channel which has the width of 5 μm and the thickness of 2 μm can be seen in Fig. 2. The channel has been isolated by the microlayer of SiO_2 from the right, left and bottom sides, where its topside covered by the thin graphene layer of 0.3 μm. The buried channel with aforesaid dimensions evidently indicates a prominent feature for the complete confinement of optical power along the Ag+ channel. The optical density profiles, which are formed in cross sections of port 1 and 2 (Fig. 2b and c), accordingly, emphasize on the approximate uniformity of the patterns within the channel as well. The graphene layer as non-metal conductor performs as a perfect blocker of power flow density and it has shown no signs of power leakage to the topside

Table 1
Fundamental mode properties.

Propagation Constant (1/μm)	Effective Index	Mode Loss (1/cm)
13.87	3.42	0.01
Group Index	Dispersion (ps/nm/km)	A_{eff} (μm^2)
3.45	−60.78	5.62

surface of the guide in Fig. 2a, whereas in SiO_2 as a substrate, the penetration of power in the regions close to port 2 is quite observable (Fig. 2c). Further consideration must be given to the phase constant of the incident wave. In the plots of optical power flow density and electric field distributions, the phase constant of zero have been taking into account and it must be noted that for the rest of phase constants and in spite of the amount of voltage/energy measured in input/output port, the best confinement can be observed in the regions highlighted by red rectangular with solid line in Figs. 2 and 3. The configuration of the waveguide doesn't allow the electric field to leak into other layers and mainly confined in Ag+ channel (Fig. 3a, b, and c). Also, the channel perfectly isolates from topside by graphene layer and no signs of electric field leakage can be observed as shown in Fig. 3a.

Dual-wavelength applications with THz spacing

In order to obtain wide passband, high quality factor and larger free spectral range optical signals, the used of coupled microring resonators is recommended [15]. These devices can be constructed in chains of micro resonators which offer a very compact and chip forms. The coupled microring resonators consist of a chain of coupled resonators in which the light can propagate within the system. In this case the light propagates by virtue of the coupling between adjacent resonators [16,17]. These systems can be used to slow down the light or manipulate the light which have many applications in optical delays, interferometers, filters, and nonlinear optics [18–21]. In Fig. 4, two MRRs are coupled to generate tunable dual-wavelength, where the first and second coupled MRRs have a radius of 6.5 and 4.5 μm respectively.

The length of the directional couplers is 25 μm and it has a coupling coefficient of 0.02. The output ports of the MRRs are shown as the through and drop ports. The system could be used for many applications in applied physics and photonics communications. The input optical field (E_i) of the Gaussian spectrum has 100 mW power. When a Gaussian input spectrum propagates within the MRR, a resonant output is formed for each round-trip [22–26]. We define the N as the number of MRRs, B as the bandwidth, f_0 is the center frequency, and $FSR = f_0/M$ (M is an integer) is the free spectral range of the MRR. The quality factor (Q factor) of each MRR can be defined as

$$Q_q = FSR/g_q B, \tag{1}$$

Where,

$$g_q = \sqrt{2} \, \sin\left(\frac{2q-1}{2N}\pi\right). \tag{2}$$

N is the number of MRRs (with q = 1 … N). The field coupling coefficients c_q of the two couplers for each MRR can be defined as

$$c_q = \frac{\pi^2}{2Q_q^2}[(1 + 4Q_q^2/\pi^2)^{1/2} - 1]. \tag{3}$$

Therefore, the c_q is not affected by the distance between two MRRs. The distance between MRRs determines the out-of-band frequency response of the MRR [27,28]. In the presented work, with circular MRRs, the distance between the MRRs is defined as

$$L_{MRR} = \frac{c}{n_{eff} FSR} = \frac{cM}{n_{eff} f_0} \tag{4}$$

The throughput output is shown in Fig. 5. Table 2 present spacing ranges between 0.29 THz and 0.95 THz. The drop output is shown in Fig. 6 and the Table 3 shows spacing ranges between 0.25 THz and 0.96 THz.

Terahertz radiation finds a large and still expanding range of applications such as communications [8], imaging [9], Spectroscopy [10], and safety Aspects [11].
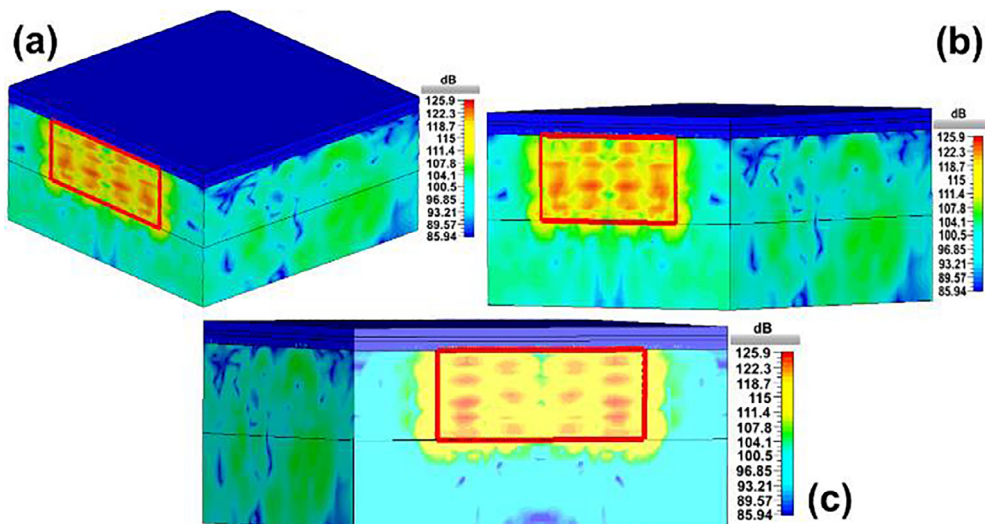
Fig. 2. Power density flows over the surface of graphene layer (a), at the input port (b) and at the output port (c) of the proposed waveguide under normal incidence excitation corresponding to λ = 1.55 μm.
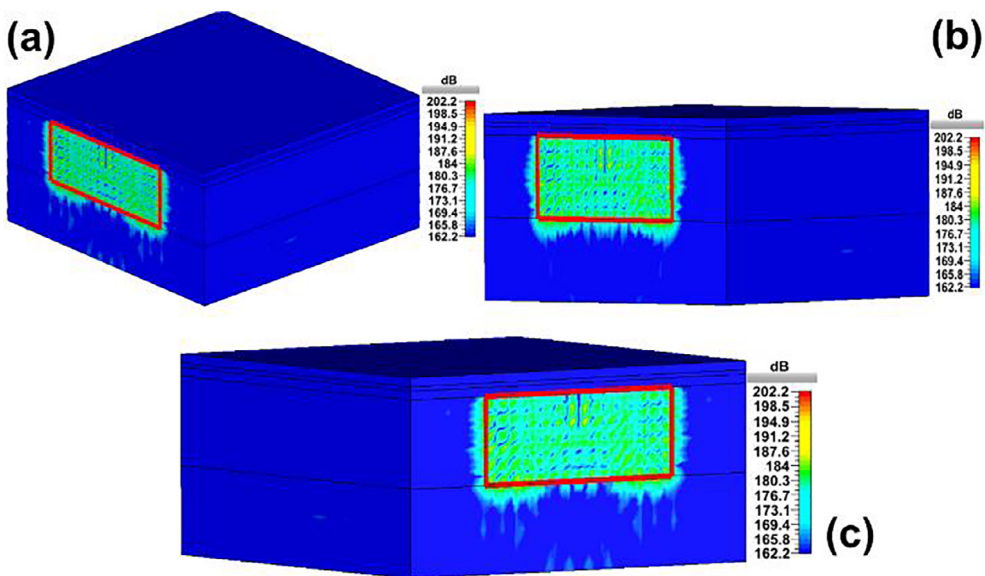

Fig. 3. The electric field distributes over the surface of graphene layer (a), at the input port (b) and at the output port (c) of the proposed waveguide under normal incidence excitation corresponding to λ = 1.55 μm.
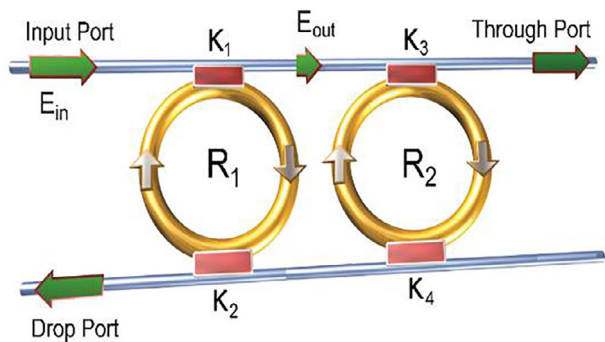

Fig. 4. Coupled microring resonators (MRRs).
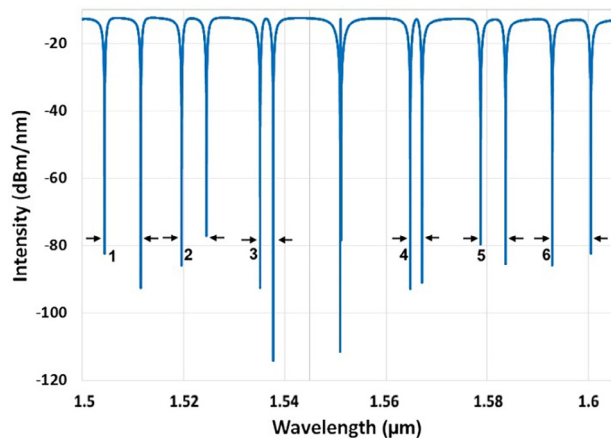

Fig. 5. Transmission simulated at the throughput port of the MRRs system.

Table 2
Throughput output, dual-wavelength spacing.

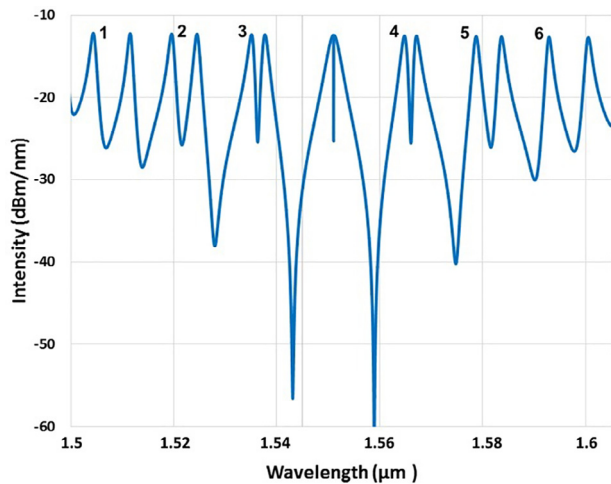| Spacing number	Spacing (nm)	Spacing (THz)
1	7.16	0.9
2	4.91	0.61
3	2.6	0.32
4	2.32	0.29
5	4.92	0.61
6	7.62	0.95

Fig. 6. Transmission simulated at the drop port of the MRRs system.

Table 3
Drop port output, dual-wavelength spacing.

Spacing number	Spacing (nm)	Spacing (THz)
1	7.3	0.91
2	4.67	0.58
3	2.47	0.3
4	2	0.25
5	5	0.62
6	7.7	0.96

Conclusion

As the conclusion, the ion exchange method is a way to produce the optical waveguide. In this performed simulation work the Ag + ion with a concentration of $0.8\,mol/m^3$ was applied to the substrates which is the glass. As mentioned earlier, controlling the Ag + concentration is the critical process, where a low concentration causes a deeper and wider junction of the waveguide. Subsequently, the MRRs system also based on glass substrates was proposed and the filtering function of the MRRs on the output optical power was analyzed. Note that the function of the system is just filtering of the input spectrum and it does not work as an active laser. The input Gaussian spectrum was spliced to many center wavelengths; therefore, the dual-wavelength were generated with spacing in the range of THz. The applications of the THz signals could be such as terahertz imaging, terahertz time-domain spectroscopy, terahertz computing/communications, and sub-mm remote sensing [29,30]. The future work will be on the fabrication and characterization of the ion exchange based MRR on glass substrates.

References

[1] Amiri IS, Ariannejad M, Ali J, Yupapin P. Design of optical splitter using ion-exchange method for DNA bio-sensor. J King Saud Univ-Sci 2018.
[2] Xia C, Li P, Li J, Jiang Q, Zhang X, Alshareef HN. General top-down ion exchange process for the growth of epitaxial chalcogenide thin films and devices. Chem Mater 2017;29:690–8.
[3] Li X, Jiang L, Li J, Mohagheghian I, Dear JP, Li L, et al. Elastic-plastic deformation in ion-exchanged aluminosilicate glass by loading rate dependent nanoindentation. J Non-Cryst Solids 2018;491:79–88.
[4] Ramaswamy RV, Srivastava R. Ion-exchanged glass waveguides: a review. J Lightwave Technol 1988;6:984–1000.
[5] Inácio PL, Barreto BJ, Horowitz F, Correia RR, Pereira MB. Silver migration at the surface of ion-exchange waveguides: a plasmonic template. Opt Mater Exp 2013;3:390–9.
[6] Nannini M, Grondin E, Gorin A, Aimez V, Broquin J-E. Hybridization of III-V semiconductor membranes onto ion-exchanged waveguides. IEEE J Select Top Quant Electron 2005;11:547–54.
[7] Scarmozzino R, Gopinath A, Pregla R, Helfert S. Numerical techniques for modeling guided-wave photonic devices. IEEE J Sel Top Quant Electron 2000;6:150–62.
[8] Part M. Combined three-dimensional sol-gel structures and atomic layer deposited thin films, 2017.
[9] Amiri IS, Ariannejad M, Kouhdaragh V, Seyedi S, Yupapin P. Microring resonator made by ion-exchange technique for detecting the CO2, H2O, and NaCl as cladding layer. J King Saud Univ-Sci 2017.
[10] Amiri IS, Ariannejad M, Ghasemi M, Naraei P, Kouhdaragh V, Seyedi S, et al. Simulation of microring resonator filters based ion-exchange buried waveguide using nano layer of graphene. J Opt 2017;46:506–14.
[11] Amiri IS, Ariannejad MM, Ahmad H, Yupapin P. A review on optical waveguide sensor using ion-exchange technology. In: Hopkins M, editor. Systems Engineering: Concepts, Tools and Applications. USA: Nova Science; 2016.
[12] Amiri IS, Ariannejad MM, Ahmad H, Yupapin P. Silver nano particle ion-exchanged glass waveguide technology. In: Hopkins M, editor. Systems Engineering: Concepts, Tools and Applications. USA: Nova Science; 2016.
[13] Ye Y, Liu X, Wang S, Liu C, Yang Y. The general effect of atomic size misfit on glass formation in conventional and high-entropy alloys. Intermetallics 2016;78:30–41.
[14] Gautam C, Manpoong C, Gautam S, Singh A, Madheshiya A, Tamuk M. Synthesis, Microstructure and Dielectric Properties of (Sr, Bi) TiO3 Borosilicate Glass-Ceramics, 2015.
[15] Schwelb O, Frigyes I. A design for a high finesse parallel-coupled microring resonator filter. Microwave Opt Technol Lett 2003;38:125–9.
[16] Yariv A, Xu Y, Lee RK, Scherer A. Coupled-resonator optical waveguide:? A proposal and analysis. Optics Lett 1999;24:711–3.
[17] Melloni A, Morichetti F, Martinelli M. Linear and nonlinear pulse propagation in coupled resonator slow-wave optical structures. Opt Quant Electron 2003;35:365–79.
[18] Poon JK, Scheuer J, Xu Y, Yariv A. Designing coupled-resonator optical waveguide delay lines. JOSA B 2004;21:1665–73.
[19] Paloczi GT, Huang Y, Yariv A, Mookherjea S. Polymeric Mach-Zehnder interferometer using serially coupled microring resonators. Opt Exp 2003;11:2666–71.
[20] Hryniewicz J, Absil P, Little B, Wilson R, Ho P-T. Higher order filter response in coupled microring resonators. IEEE Photonics Technol Lett 2000;12:320–2.
[21] Heebner JE, Chak P, Pereira S, Sipe JE, Boyd RW. Distributed and localized feedback in microresonator sequences for linear and nonlinear optics. JOSA B 2004;21:1818–32.
[22] Amiri I, Soltanian M, Alavi S, Ahmad H. Multi wavelength mode-lock soliton generation using fiber laser loop coupled to an add-drop ring resonator. Opt Quant Electron 2015;47:2455–64.
[23] Alavi S, Amiri I, Ahmad H, Supa'at A, Fisal N. Generation and transmission of 3× 3 w-band multi-input multi-output orthogonal frequency division multiplexing-radio-over-fiber signals using micro-ring resonators. Appl Opt 2014;53:8049–54.
[24] Amiri I, Ali J. Optical quantum generation and transmission of 57–61 GHz frequency band using an optical fiber optics. J Comput Theor Nanosci 2014;11:2130–5.
[25] Amiri I, Ali J. Generating highly dark–bright solitons by Gaussian beam propagation in a PANDA ring resonator. J Comput Theor Nanosci 2014;11:1092–9.
[26] Amiri I, Alavi S, Soltanian M, Fisal N, Supa'at A, Ahmad H. Increment of access points in integrated system of wavelength division multiplexed passive optical network radio over fiber. Sci Rep 2015;5:11897.
[27] Soltanian M, Amiri IS, Alavi SE, Ahmad H. All optical ultra-wideband signal generation and transmission using mode-locked laser incorporated with add-drop microring resonator (MRR). Laser Phys Lett 2015;12.
[28] Amiri IS, Alavi SE, Soltanian MRK, Fisal N, Supa'at ASM, Ahmad H. Increment of access points in integrated system of wavelength division multiplexed passive optical network radio over fiber. Sci Rep 2015;5.
[29] Afroozeh A, Amiri I, Samavati A, Ali J, Yupapin P. THz frequency generation using MRRs for THz imaging. In: Enabling Science and Nanotechnology (ESciNano), 2012 International Conference on, 2012, pp. 1–2.
[30] Amiri I, Ahmad H, Ghasemi M, Ismail M, Aidit S, Soltanian M, et al. Silicon-based microring resonators for multi-solitons generation for THz communication. Opt Quant Electron 2016;48:415.